Chapter 4

IMPACT OF URBAN STRETCH ON THERMAL PATTERN OF THE RIVER

4.1 Introduction

Anthropogenic activities like industrial discharge, domestic sewer discharge, and agricultural run-off considerably affect the river temperature, which in turn affects the aquatic ecosystem (Caissie, 2006; Ling et al., 2017; Smith, 2008; Wawrzyniak et al., 2011). Water quality parameters like dissolved oxygen (DO), pH, salinity, and suspended sediment concentration depend on river water temperature. Numerous biological factors are also one of the reasons for the water temperature variation of the rivers. Stream temperature becomes an important factor in water quality, predominantly in those areas where endangered fish species are sensitive to water temperature flux (Handcock et al. 2006). The physical, chemical, and biological properties of rivers are also affected by stream temperatures; it affects aquatic organisms' metabolic rates and life histories, the efficiency of chemical reactions, DO concentrations, and nutrient cycling. DO concentration also influences the metabolic rates of amphibian life forms and predation hazard, impacting the creature behavior and fish network structures (Magoulick and Kobza, 2003; Null et al., 2017; Poole and Berman, 2001).

Variations of water temperature in the river can occur naturally or as a result of anthropogenic activities, such as point source and non-point source pollutant discharge from industrial, commercial, housing, and agricultural sectors. It can ultimately affect fisheries and aquatic

resources (Caissie, 2006). Atmospheric conditions also play an important role in heat exchange processes at the water surface, incorporating phase changes. Deforestation has been distinguished as a critical parameter in influencing the river thermal system (Beschta, 1997; Brown and Krygier, 1970; Caissie, 2006; Ling et al., 2017). Potential stream channel modification can likewise be in charge of changes in river water temperature (Morse, 1972; Sinokrot and Gulliver, 2000). Global climate change has been a concern for environmentalists in recent times. With the rise in the temperature globally, the water temperature is also warming worldwide (Schindler, 2001; Sinokrot et al., 1995; Richards et al., 2018).

The increment in water temperature doesn't follow a straightforward relationship, and the increment rate is more noteworthy for small streams than big rivers (Caissie, 2006). The morphology of rivers can also influence thermal patterns; braided streams can encounter high water temperatures because of their shallow channels exposed to meteorological conditions (Caissie,2006; Mosley, 1983). In general, the thermal patterns of rivers are greatly affected by local climate, river conditions (physical, chemical, and biological), and geographical settings (Caissie, 2006). As there is an increasing consciousness about the effect of global warming in the aquatic ecosystem, so the study about the temporal and spatial pattern of river temperature becomes significant for the fluvial scientist and ecologists working on the river ecosystem (Carpenter et al., 1992; Flebbe et al., 2006; Mohseni et al., 2003; Wawrzyniak et al., 2011).

Early investigations of river water temperatures primarily concentrated on habitat use by aquatic plants and animals (Gibson, 1966). At this juncture, remote sensing is a very useful substitute, as images from the satellites have a large spatial extent. Their periodic movement over the same area can be useful in temporal studies. Sensors of the satellite can catch the

radiation energy of the different earth features in the visible region as well as the non-visible region of the electromagnetic (EM) spectrum.

Through a Landsat program, fluvial research has attained a new dimension. However, analysis of water temperature was not given due attention (Baban, 1993; Frazier and Page, 2000; Kay et al. 2005; Wawrzyniak et al. 2011). The objective of the present chapter is to investigate temporal and spatial thermal patterns of the Ganga river at Varanasi (an important segment of the stretch selected for the present study) and nearby places with the help of Landsat-8 satellite images. In addition to this, the accuracy evaluation of the temperature values generated from the satellite images has also been performed by recording in-situ temperature values using the portable thermal sensor.

Varanasi is a city located on the left bank of the Ganga river. The river flowing through this region is highly polluted. The significant sources of pollution are effluents discharging from industries and sewage generated from domestic wastes. Approximately there are around 1500 industries located in and around the Varanasi region, such as the textile and leather industry, chemical industry, and metal processing industries (Mishra and Tripathi, 2008; Rai and Tripathi, 2008; Das et al., 2022). Large quantities of chemical fertilizers and insecticides are used on the uninhabited right bank of the river to raise agricultural crops; during rainfall and flooding, these toxic substances pass over to the river. These activities are enhancing the pollution level in the region.

As shown in Figure 4.1, three confluence points were chosen to analyze the water temperature variation due to the discharge of effluents into the river Ganga. Its description is given in Table 4.1. Some mid-Ganga points were also selected for estimating mid-river temperatures along with these confluence points. Mid Ganga point, which is nearest to the reference point, is

depicted as M1. All the other points have been marked in a similar order (for example, mid-Ganga point situated near Industrial outlet is M2 and so on). It might be stated that this reference point has been selected for estimating the relative water temperature variation.

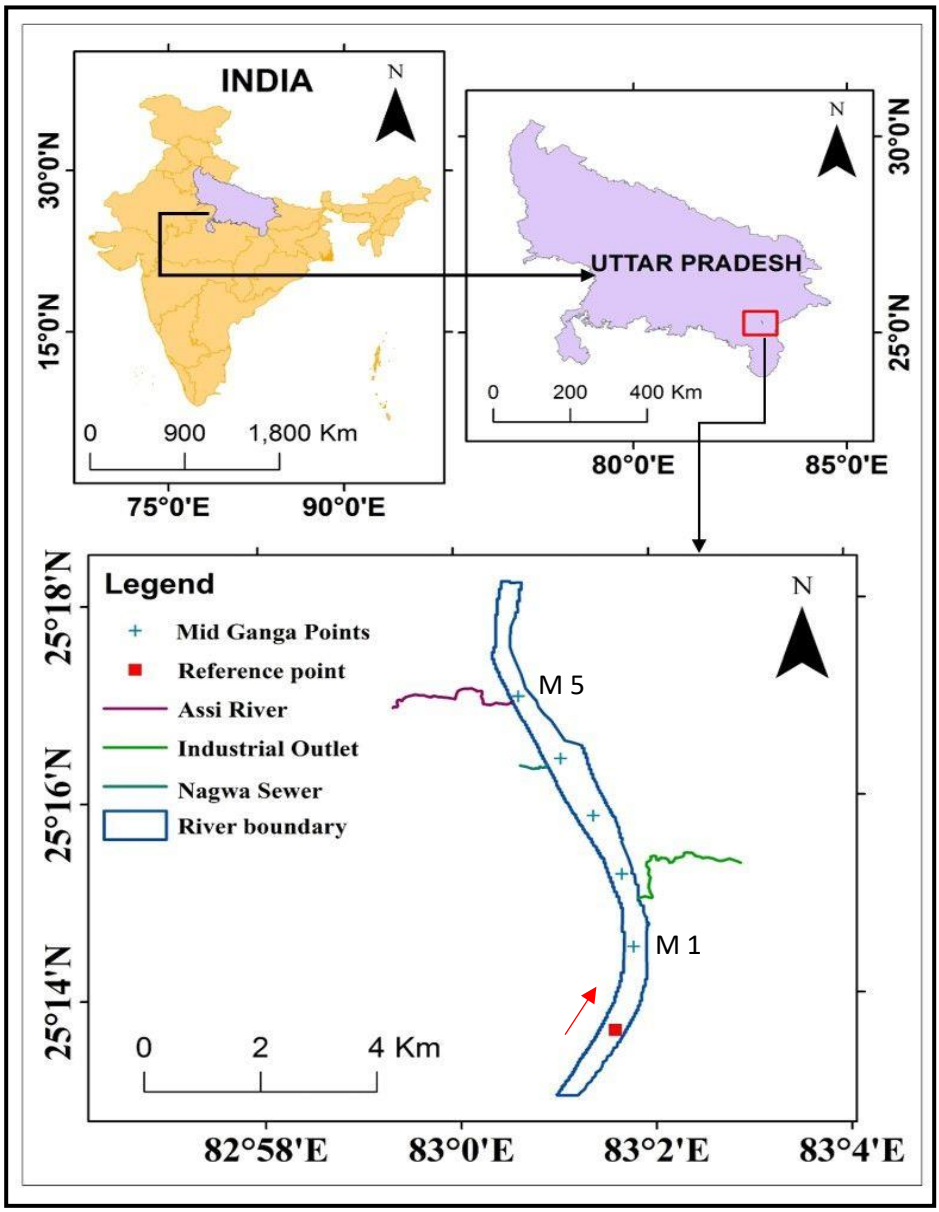

Figure 4.1 Location map showing the confluence points

The characteristics of the three confluence points are given in Table 4.1.

Table 4.1: Characteristics of the confluence points

S.No.	Name of the Confluence point	Nature of Discharge
1	Assi river outlet(C1)	Domestic and commercial sewage discharge in a huge amount
2	Nagwa sewer outlet (C2)	Domestic sewage discharge
3	Industrial outlet near DGPS station (C3)	Domestic as well as industrial discharge

4.2 Data

The LANDSAT-8 datasets have been used, and 23 cloud-free images have been processed between June 2013-November 2020. The Landsat scenes selected for the study area were of path 142/ row43. The chosen Landsat scenes were, between the years 2013 to 2018, having almost 0% cloud cover and were freely downloaded from the United States Geological Survey Earth Explorer site (http://earthexplorer.usgs.gov). All the images were Level 1T products, which have been precision and terrain corrected in GeoTIFF format and are in the UTM Zone 44N projection and WGS-84 as an ellipsoidal datum (Reuter et al., 2015).

Table 4.2: Summary of satellite datasets used

Datasets	Period of the analysis	Description
Landsat-8	June 2013 – November 2020 (n=23)	Green (B-3) and NIR (B-5) bands (30 m); TIR band -10 (100 m)

4.3 Materials and Method

In this work, an attempt has been made to monitor the thermal patterns in the river Ganga at the Varanasi stretch. The analysis was done by using Landsat 8 time-series images from 2013-2020, and the steps are shown in Figure 4.2.

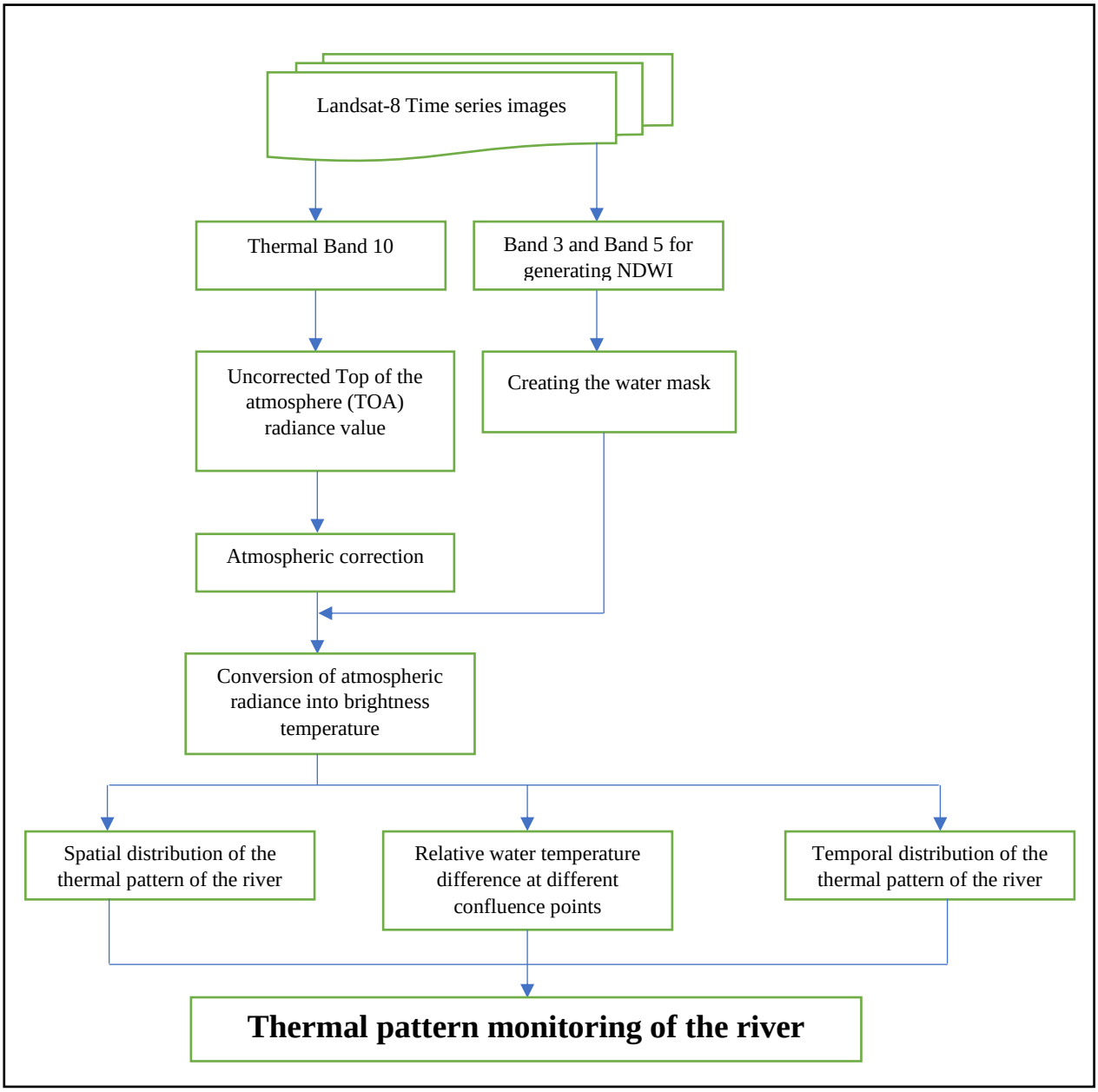

Figure 4.2 Flowchart of the work

4.3.1 Portable thermal sensor

The sensing gadget consists of hardware and software parts. The hardware portion includes the temperature sensor "TSY01," which is connected to an Arduino microcontroller, and Bluetooth is also attached to this system for data transfer. This whole system has been supplied with power for its functionality with the help of a power bank, which is portable in nature (Daigavane and Gaikwad, 2017; Das et al., 2019). This portable thermal sensor can be commanded with the help of a mobile app, and the temperature which is recorded with this sensor can be kept in the app itself as a text file. The text file which is generated by the app can be transported to the ArcGIS environment for visualization. Pre-calibration of this gadget has been done by MEAS company, based in the USA, and has an accuracy of±0.1°C. The Block diagram for this sensor system is shown in Figure 4.3, and the complete sensor system setup is depicted in figure 4.4. This portable setup for measuring the in-situ temperature of the river has several advantages over temperatures recorded at hydrological stations. With the help of a portable thermal sensor, one can measure the in-situ temperature approximately at the same time when there is a satellite overpass, but the hydrological stations are limited to measuring temperatures at fixed timings. So, there will be more variation between the in-situ temperatures recorded at the hydrological station than temperatures estimated from the satellite; as this variation increases, the uncertainty in results will be enhanced. Another advantage of having the portable setup is that one can take several points in the study area chosen for in-situ measurement; this reduces the uncertainty and RMSE (Root Mean Square Error) value between the estimated and observed temperatures.

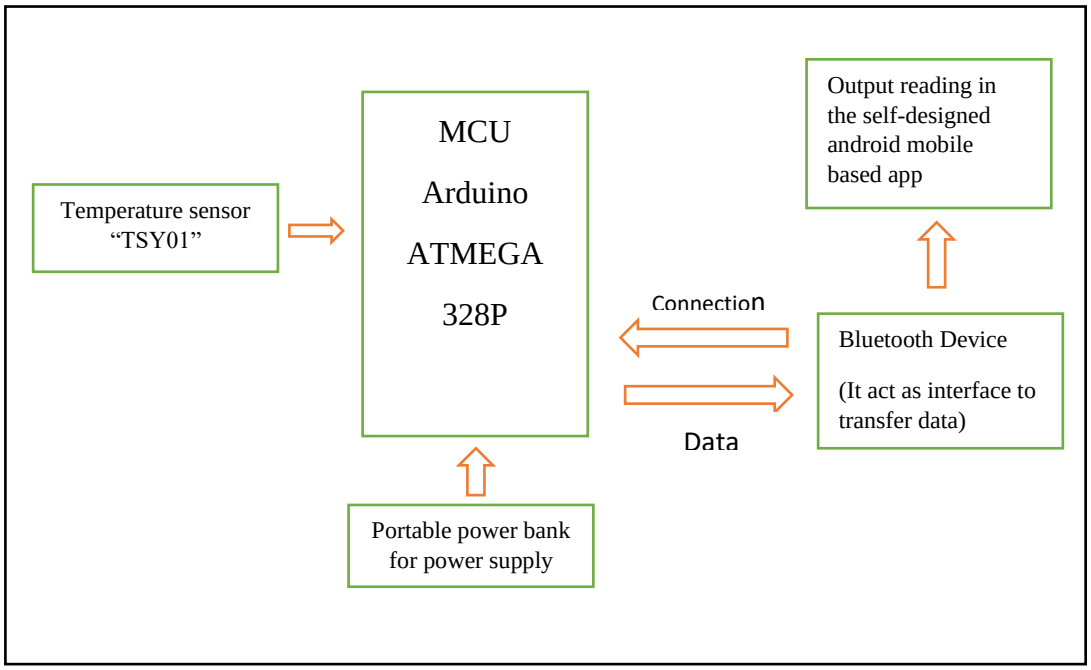

Figure 4.3 Functional block diagram of the sensor system set-up

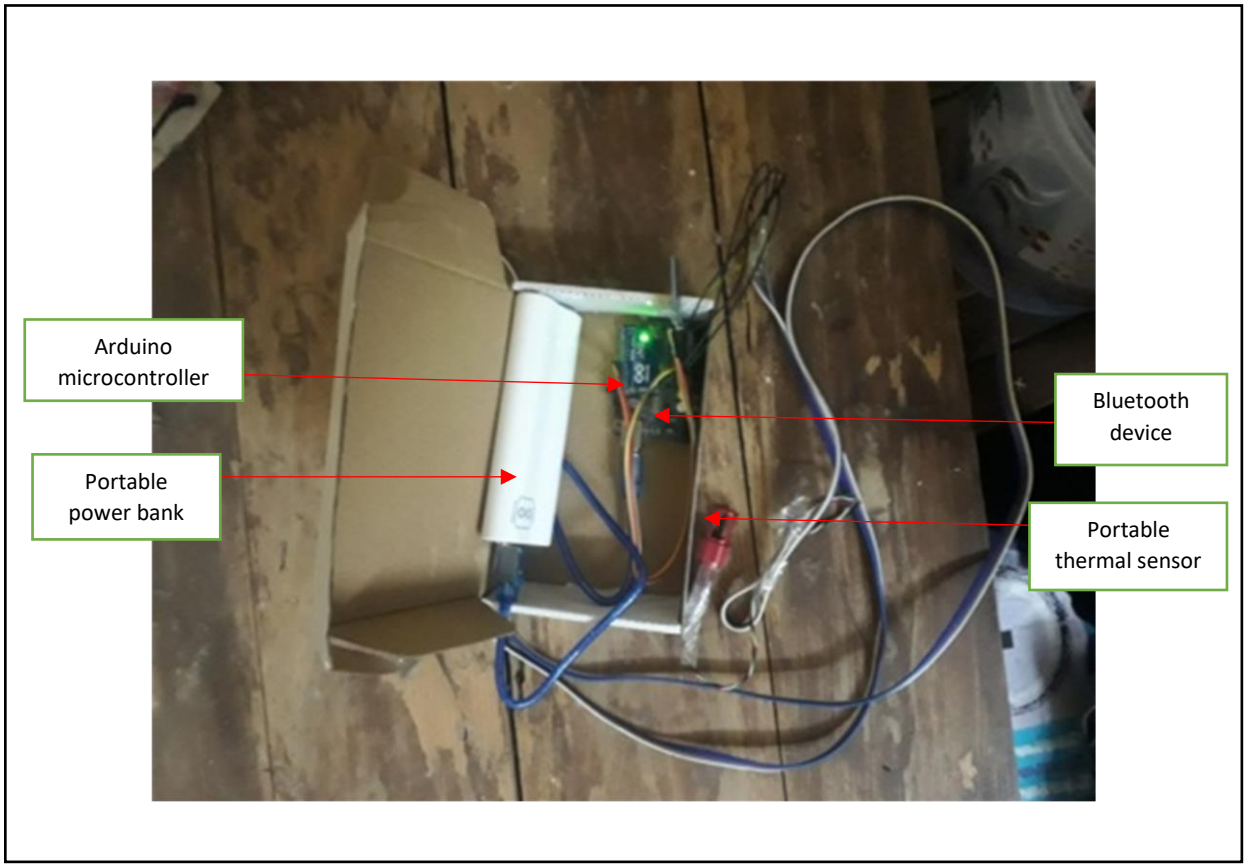

Figure 4.4 Portable sensor system set up

4.4 Results

4.4.1 Validation of Estimated Water Temperature

For the validation of the temperature calculated from satellite images, the results were compared with the values of water temperature observed through the portable sensor system. For this purpose, six images were selected whose acquisition dates are 25th December 2018, 10th January 2019, 11th February 2019, 4th March 2021, 20th March 2021, 5th April 2021 respectively and scene IDs are "LC08_L1TP_142043_20181225_20190129_01_T1", "LC08_L1TP_142043_20190110_20190131_01_T1", "LC08_LITP_142043_20190211_20190222_01_T1" , "LC08_L1TP_142043_20210304_20210312_02_T1", "LC08_L1TP_142043_20210320_20210328_02_T1", "LC08_L1TP_142043_20210405_20210409_02_T1" respectively. Since the satellite overpass through the study area was known beforehand from the Landsat overpass calendar issued by USGS along with the approximate overpass time, the in-situ data were recorded for several points in the study area for the overpass dates. Around 120 sample points were chosen along both the banks and mid-section of river Ganga, for which in-situ temperature was measured, and a good correlation along with RMSE value of 0.956 was observed, as shown in figure 4.5. To mark the coordinates of the points, "Garmin Etrex 30" GPS system was used. The Garmin Etrex 30 is accurate to 3 meters. This means the GPS will give the location at any given time within 3 meters of the actual location. The GPS device saves the point (LAT &LONG) in degrees, minutes, and seconds format, e.g., 34º26'31.73" N and 74º09'14.38"E. But this format needs to be converted into degree decimal, e.g., 34.442N and 74.153E. The ArcGIS software was applied for plotting these points on the layer which has already been created in this software, and this layer comprises the temperature of the water surface. Thus

with the help of the “extract value to points” tool of the above-mentioned software, the temperature values of these plotted points have been acquired. These points will now show some temperature values as an attribute, which can be seen in the software itself, and those values are satellite-determined temperatures. These temperature values are computed with the steps written in the ‘*surface water temperature calculation’* section (section 3.4.3) in chapter 3. For each satellite overpass day, 20 in-situ temperature points have been recorded for the satellite-derived temperature validation. On the map, 20 in-situ points location has been shown. For all six sampling days, the in-situ temperature has been measured at these places. Figure 4.6 shows the in-situ temperature measurement points.

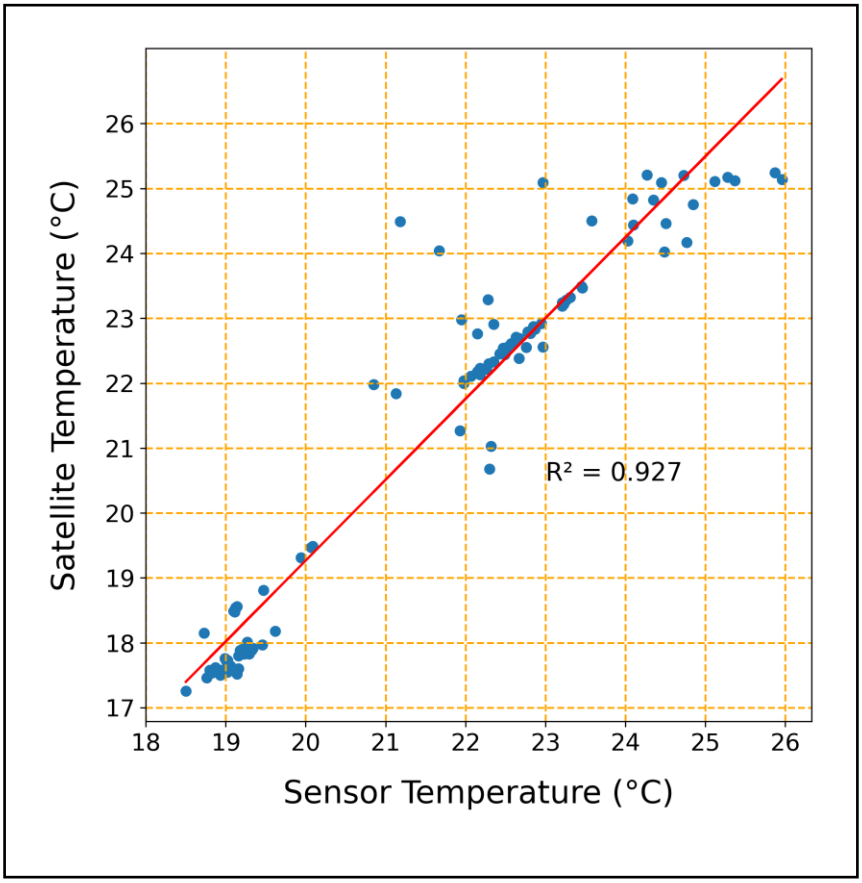

Figure 4.5 Correlation graph between the temperature observed from the portable thermal sensor and satellite-derived temperature

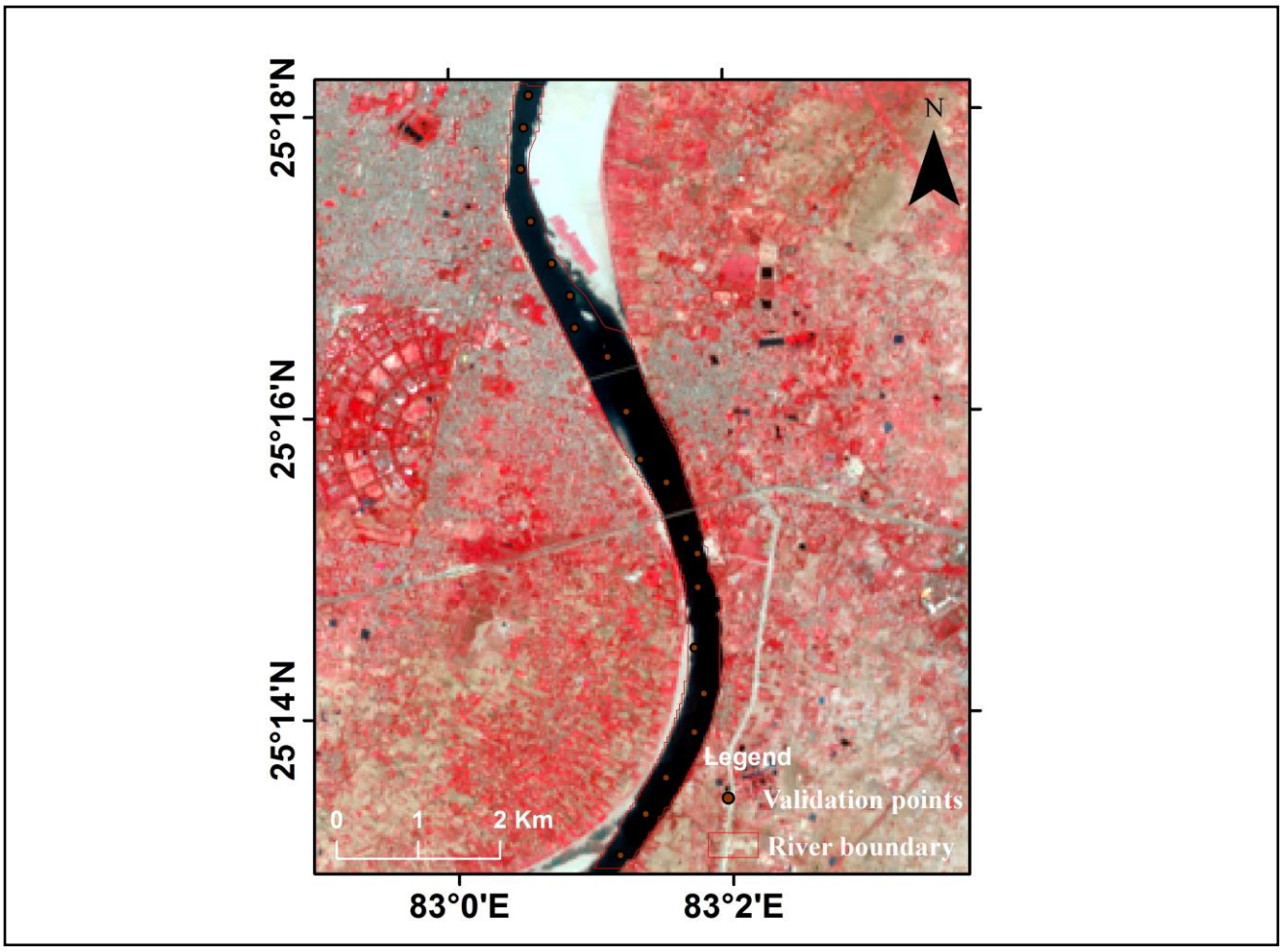

Figure 4.6 Map of the in-situ temperature measurement point

4.4.2 Spatio-temporal Variation of River Thermal Profile

4.4.2.1 Spatial variation of River Water Temperature

The temperature map has been prepared from the satellite image, as shown in figure 4.7. The map depicts the spatial variation of river surface temperature over the study area. The river stretch in the figure is around10 kilometers long; its width varies from 230 to 700 meters over the stretch and flows in the north direction. As it is such a wide river, the effect of effluent discharge is not visible on the thermal map with a coarse resolution.

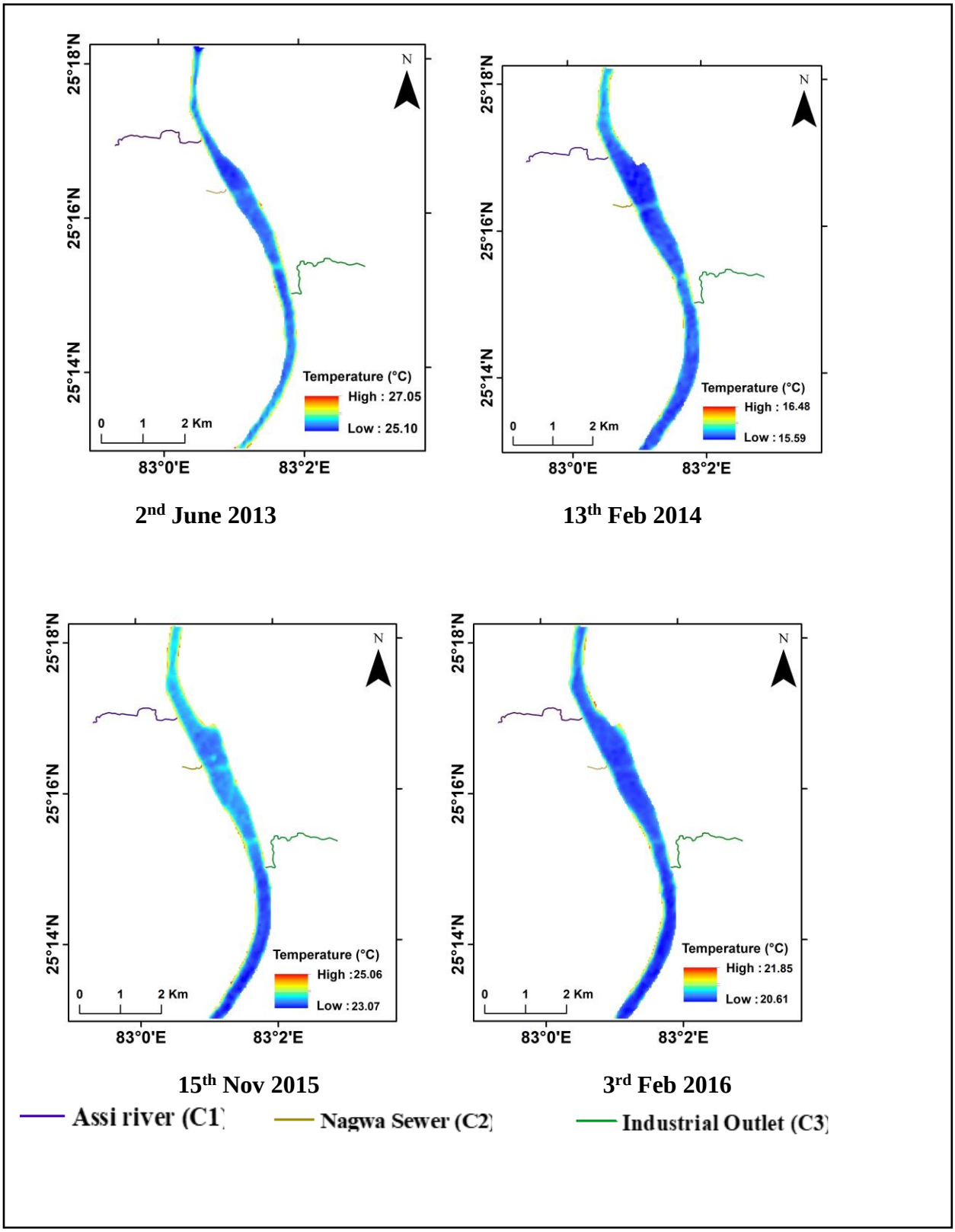
25°18'N
25°16'N
25°14'N
N
Temperature (°C)
High : 27.05
Low : 25.10
0 1 2 Km
83°0'E
83°2'E
2nd June 2013
Temperature (°C)
High : 16.48
Low : 15.59
13th Feb 2014
Temperature (°C)
High :25.06
Low : 23.07
15th Nov 2015
Temperature (°C)
High : 21.85
Low : 20.61
3rd Feb 2016
Assi river (C1)
Nagwa Sewer (C2)
Industrial Outlet (C3)

Contd.

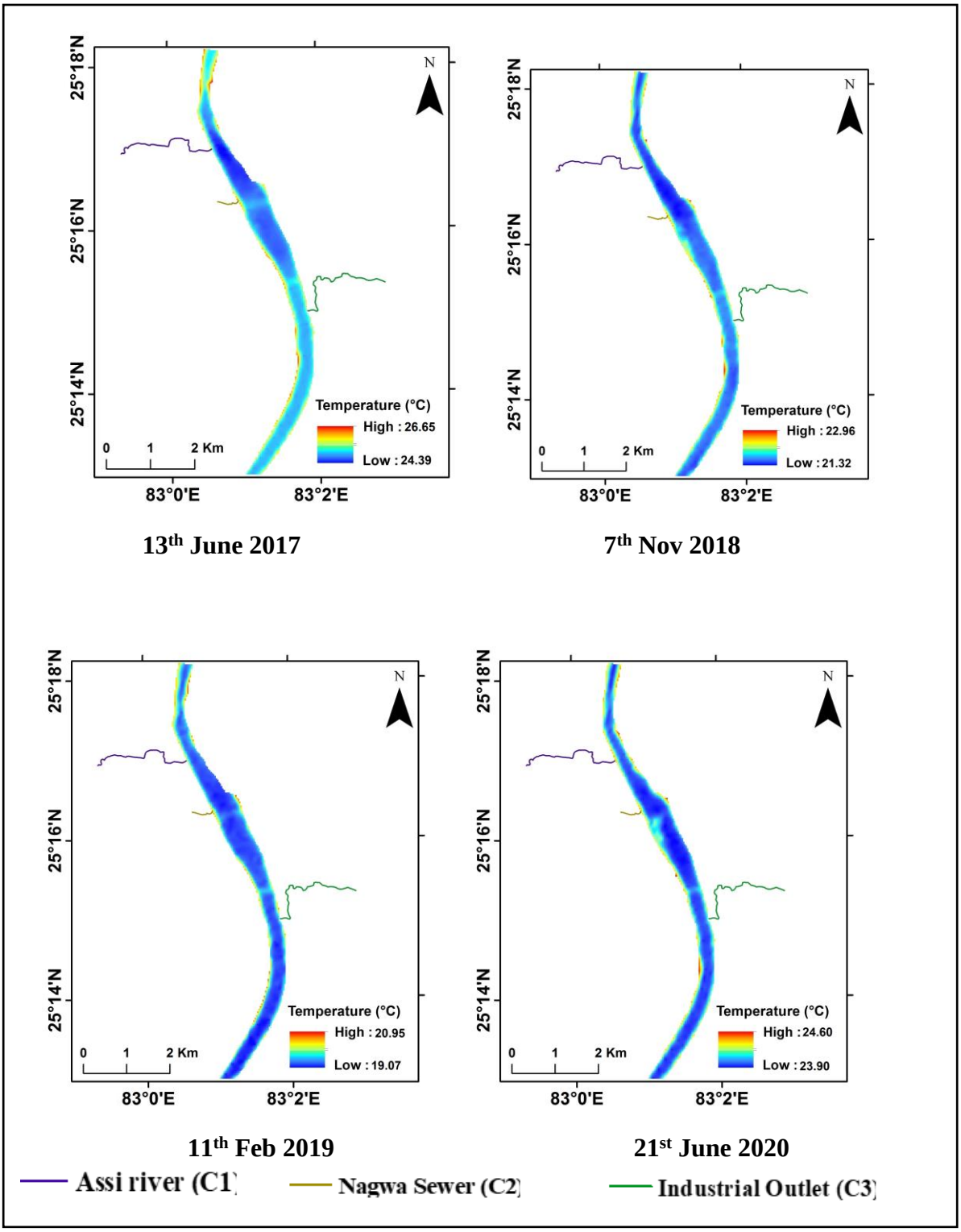

Figure 4.7 Spatial distribution of river thermal profile

The exact location for the river thermal pattern variation due to the confluence points is tough to detect on a map of such scale. Two images, i.e., Feb 2019 and Nov 2018, have been chosen, and the zoom scale representation for some pixels near confluence point (s) has been shown.

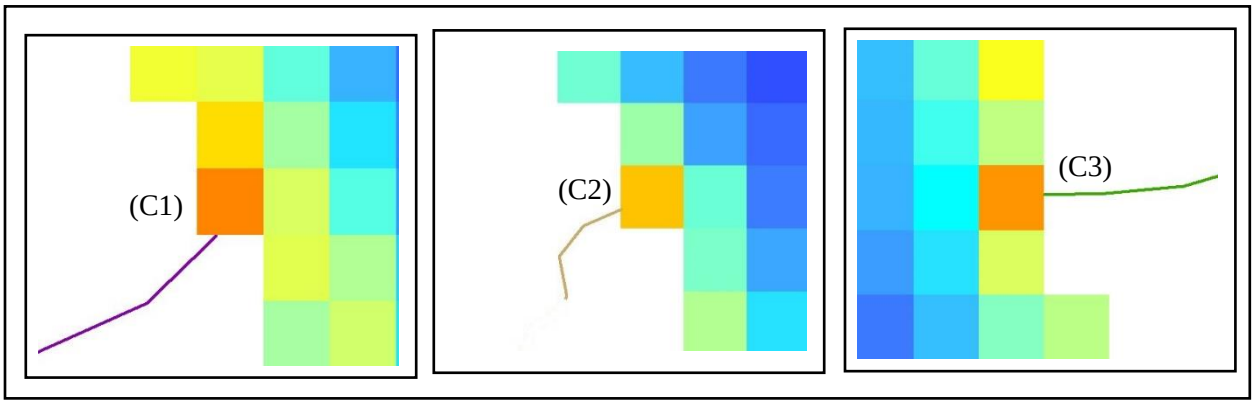

Figure 4.8 February 2019 image depicting confluence point variation

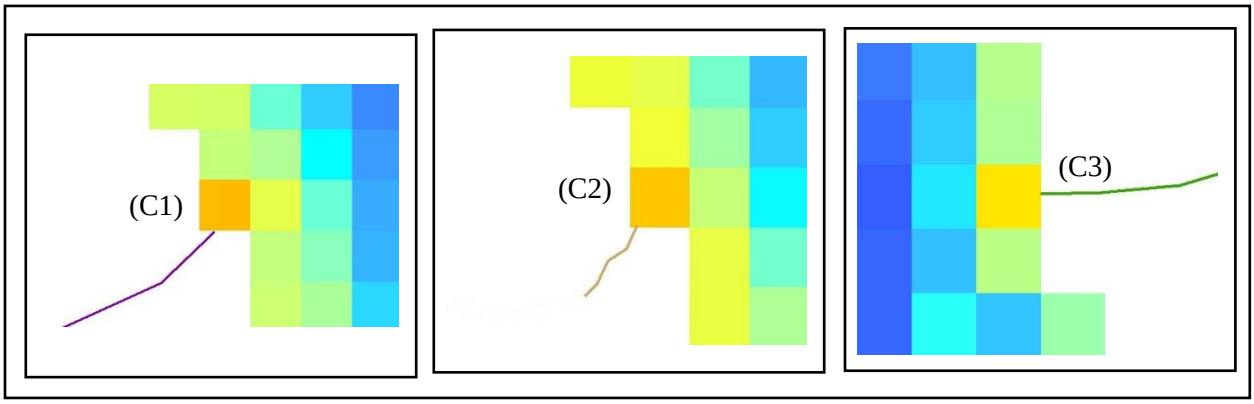

Figure 4.9 November 2018 image depicting confluence point variation

But a gradual pattern of thermal variation over a range of temperatures can be observed from the images. The variations generally remain low for February and November months and high during June. It was also observed that water temperatures along the bank were relatively higher than in the mid-section. To get a better idea of the spatial variation of temperature over the stretch, a tabular form of representation is also given in Table 4.3. Temperature values are in degrees Celsius (°C).'C' depicts the confluence points, and 'M' depicts the mid-Ganga points shown as a plus (+) sign in figure 4.1.

Table 4.3. Spatial variation of river temperature

Year and Month	C 1	C 2	C 3	M 1	M 2	M 3	M 4	M 5	Min Temp	Max Temp	Ref. pt. Temp
2013 June	26.75	26.68	26.71	25.12	25.28	25.19	25.31	25.23	25.10	27.05	25.55
2014 Feb	16.37	16.35	16.29	15.62	15.67	15.89	15.88	15.85	15.59	16.48	15.60
2015 Nov	24.82	24.80	24.76	23.97	23.98	23.13	23.19	23.12	23.07	25.06	23.08
02016 Feb	21.78	21.76	21.71	20.62	20.62	20.64	20.73	20.75	20.61	21.85	20.61
2017 June	26.42	26.41	26.35	25.10	25.03	24.97	24.42	24.45	24.39	26.65	25.12
2018 Nov	22.65	22.60	22.41	21.32	21.68	21.61	21.52	21.70	21.32	22.96	21.34
2019 Feb	20.72	20.74	20.65	19.32	19.29	19.29	19.21	19.16	19.07	20.95	19.07
2020 June	24.35	24.31	24.09	23.92	23.95	23.94	23.95	23.95	23.90	24.60	23.90

It is clearly evident from Table 4.3 that temperature at all three confluence points remains higher throughout the study period than mid-Ganga region. This indicates that effluent discharge into a large river has little influence on the overall river temperature, and its effect can only be observed along the banks, some meters downstream of the confluence. The variation between confluences and the mid-Ganga region increases during the month of June and remains relatively less during February and November.

4.4.2.2 The relative water temperature difference in comparison to the reference point

A reference point has been chosen to calculate the river's relative water temperature variation (Ling et al. 2017). The point is chosen on the river, where it is in pristine condition. So, in this case, the reference point has been selected on the river before it enters Varanasi city, and it has been assumed that the river water at this point is fresh and clean. There is no confluence point nearby the reference point. So this point will not be influenced by sewer discharge. The reference point temperature is assigned as zero value in all the cases, and the temperature values are in °C.

Table 4.4 Relative surface water temperature variation for the year 2013

	June (2 June)	November (9 Nov)
Confluence Pt. 1	1.2	1.27
Confluence Pt. 2	1.13	1.22
Confluence Pt. 3	1.16	1.19

Table 4.5 Relative surface water temperature variation for the year 2014

	February (13 Feb)	June (5 June)	November (12 Nov)
Confluence Pt. 1	0.77	1.71	1.79
Confluence Pt. 2	0.75	1.67	1.76
Confluence Pt. 3	0.69	1.60	1.72

Table 4.6 Relative surface water temperature variation for the year 2015

	February (16 Feb)	June (8 June)	November (15 Nov)
Confluence Pt. 1	1.78	1.67	1.74
Confluence Pt. 2	1.74	1.66	1.72
Confluence Pt. 3	1.72	1.62	1.68

Table 4.7 Relative surface water temperature variation for the year 2016

	February (3 Feb)	June (10 June)	November (17 Nov)
Confluence Pt. 1	1.17	1.58	1.62
Confluence Pt. 2	1.15	1.57	1.60
Confluence Pt. 3	1.10	1.52	1.59

Table 4.8 Relative surface water temperature variation for the year 2017

	February (21 Feb)	June (13 June)	November (4 Nov)
Confluence Pt. 1	1.14	1.3	1.46
Confluence Pt. 2	1.13	1.29	1.43
Confluence Pt. 3	1.09	1.23	1.41

Table 4.9 Relative surface water temperature variation for the year 2018

	February (24 Feb)	June (14 June)	November (7 Nov)
Confluence Pt. 1	1.31	1.27	1.31
Confluence Pt. 2	1.28	1.23	1.26
Confluence Pt. 3	1.08	1.06	1.07

Table 4.10 Relative surface water temperature variation for the year 2019

	February (11 Feb)	June (18 June)	November (14 Nov)
Confluence Pt. 1	1.65	1.61	1.64
Confluence Pt. 2	1.67	1.59	1.61
Confluence Pt. 3	1.58	1.56	1.58

Table 4.11 Relative surface water temperature variation for the year 2020

	February (14 Feb)	June (21 June)	November (11 Nov)
Confluence Pt. 1	1.63	0.45	0.97
Confluence Pt. 2	1.61	0.41	0.81
Confluence Pt. 3	1.59	0.19	0.39

From Tables 4.4-4.11; it is clear that temperatures at the confluences are relatively higher for all the years. All the confluence points were within a range of seven kilometers downstream from the reference point. Amongst all the confluence points considered for the study, 'Confluence Point 3' had the least relative temperature variation for the selected years. This is

due to the fact that the source of pollution (i.e., some industries like paper and pulp, metal) is located at a distance from the point of confluence. The industry treats its waste before discharging it into the sewer. ‘Confluence Point 2’ shows the maximum temperature fluctuation of 1.77°C for February and June 2014. This has been the maximum relative temperature variation. During the months of June, the reference point has a higher temperature value as compared to the mid-Ganga points (M1-M5). This may be because the region where the reference point has been placed, the river, is narrow in that region. In addition, the presence of sandbars (an important geomorphic feature in the area) in that region further elevates the water temperature, particularly in the summer region. The sandbars get extremely heated in summer due to low thermal inertia, and in turn, it heats the river nearby to a great extent. Due to this, the reference point has elevated temperature in June as compared to February and November. This may be one of the probable reasons for the low relative temperature variation in June as compared to February. In June 2020, there has been a minimal variation of relative surface water temperature for three confluence points. During this period, the country was in the grip of the lockdown phase imposed by the government due to the COVID-19 pandemic. Due to the lockdown, most industries have been closed, so the industrial waste discharge was also very low in this period. So the river nearby the confluence point becomes significantly less polluted, and the temperature difference is minimal.

4.4.2.3 Temporal variation of River Water Temperature

The temporal variation of temperature over the years has been shown in figure 4.10, figure 4.11, and figure 4.12 for all three confluence points.

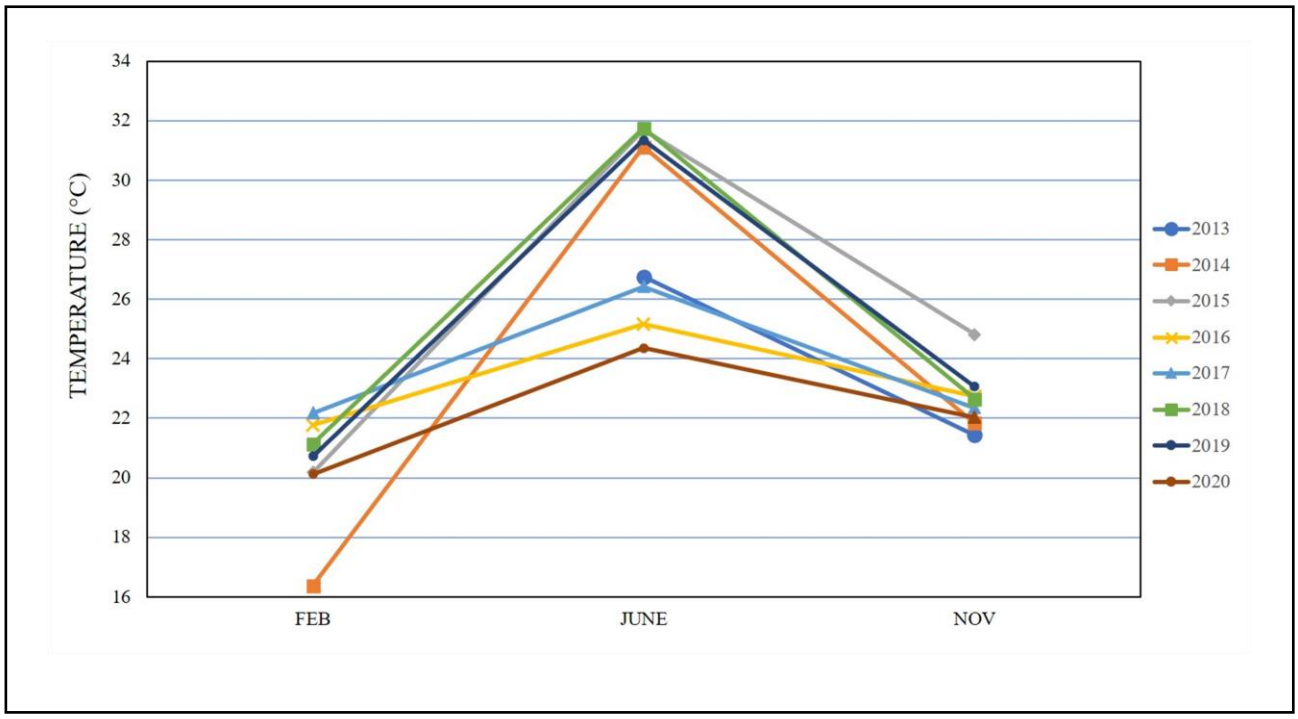

Figure 4.10 Temporal temperature profile graph for Confluence Point 1

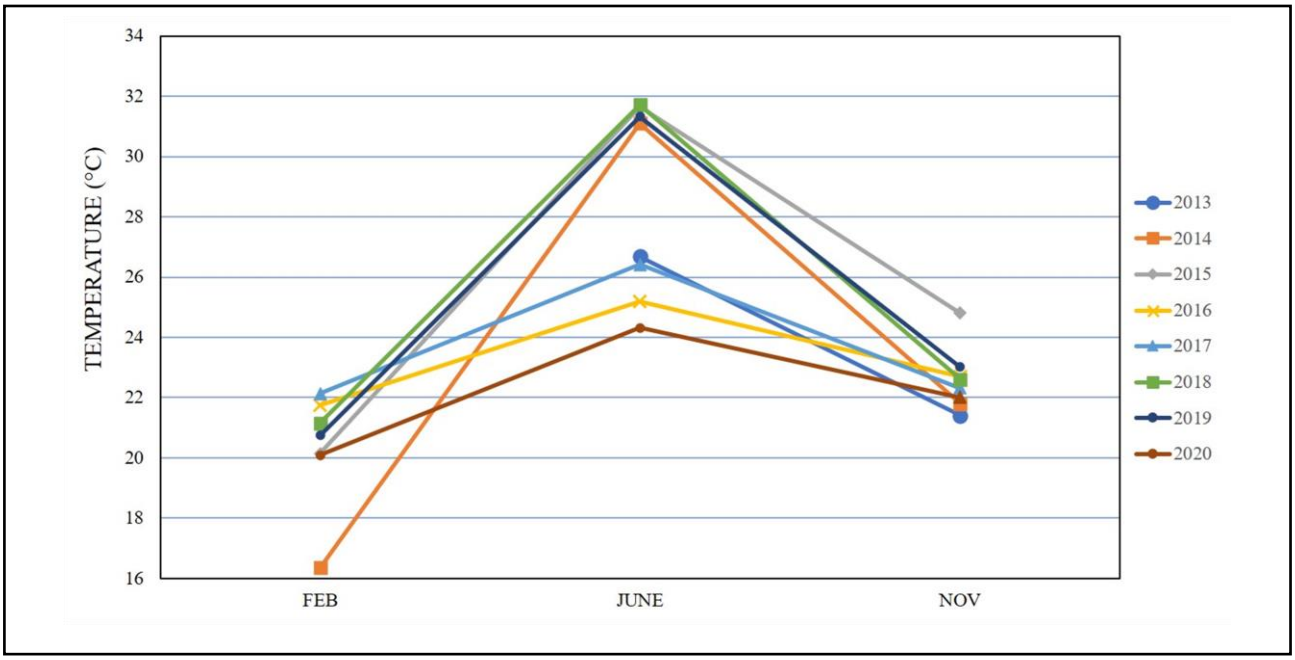

Figure 4.11 Temporal temperature profile graph for Confluence Point 2

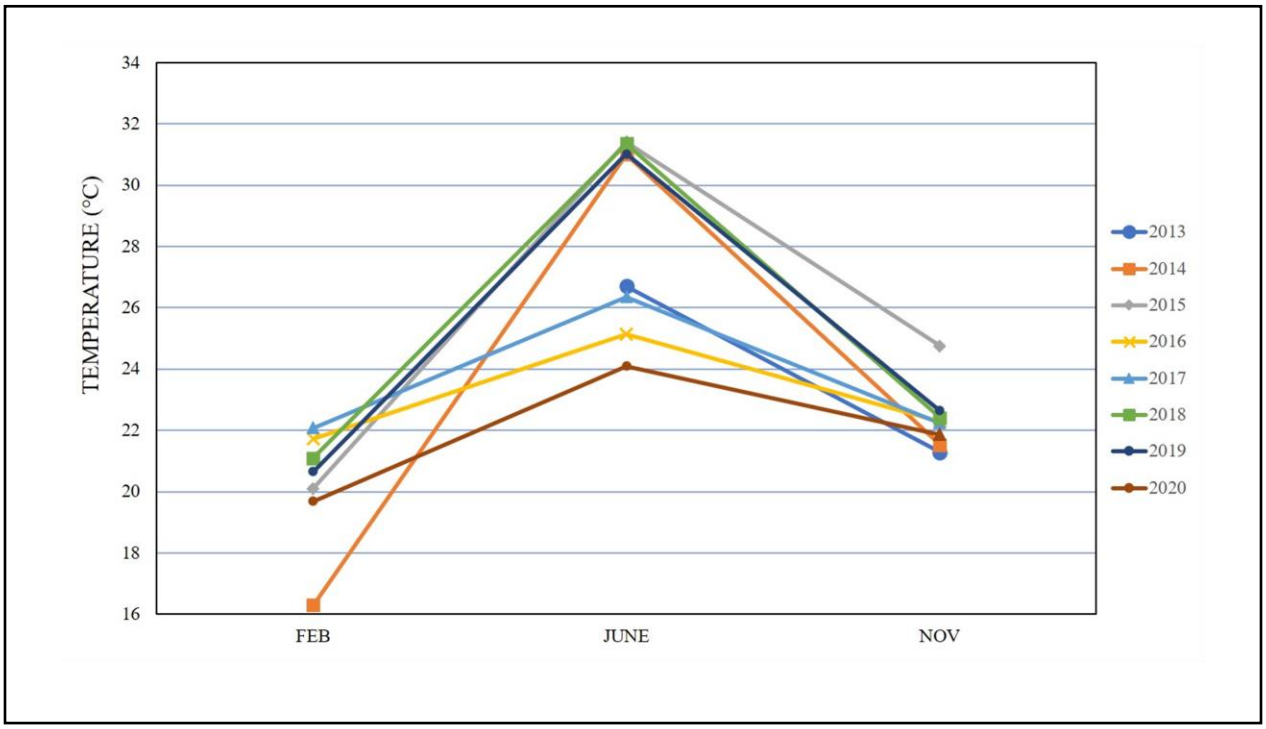

Figure 4.12 Temporal temperature profile graph for Confluence Point 3

Over the years, all three confluences show a similar trend in temperature variation for the given months, with temperatures rising sharply from February to June and then gradually decreasing from June to November. The maximum temperature was observed in June 2014 for 'Confluence points 1 and 2' and in June 2017 for the 3rd point. Temperature values for June 2016 for all three points were abnormally low compared to the rest of the years. For the 'Confluence points 1 and 2', February 2014 has the lowest February-season temperature, and February 2017 has the highest February-season temperature. The 'Confluence point 3' has the highest February-season- the temperature in February 2016. All three confluence points represent the highest November-season- temperature during November 2015. There was no data available for February 2013 as the satellite images of Landsat-8 were released by USGS in March 2013.

4.5 Discussion

With the analysis of temporal and spatial variation of the thermal pattern of the river, in the considered stretch, with the help of the Landsat-8 satellite, it can be seen that confluence points and their adjoining areas have higher temperature differences in comparison to mid-Ganga surface temperature. Point source pollutants may introduce lateral heterogeneities. In this work, alterations in the temperature caused by metrological and hydrological conditions are not taken into account. In general, the magnitude of thermal variation caused by effluents discharge at the confluence points in summer is more than that in winter. From the temporal variation graph, we can also see that the June 2016 temperature was significantly lower for all three confluence points than in other years. One reason for this difference may be attributed to different meteorological and hydrological conditions existing during that period. However, further studies on the role of meteorological and hydrological factors vis-a-vis thermal variation on the river ecosystem are desired. In June 2020, the river temperature was relatively lower than other June seasons (except June 2016). This could be attributed to the fact that the country was under lockdown during that period (Garg et al., 2020). The industries were primarily closed, which reduced the carbon emission. The concentrations of PM_{10} and $PM_{2.5}$ have witnessed the maximum reduction. Due to the carbon emission depletion, the air temperature gets decreases (Mahato et al. 2020). The air temperature directly relates to water temperature (Webb, 1996), so water temperature also depicts a lowering trend during that period. This work also analyzes the spatial extent of thermal patterns in the river Ganga. With all the freely available Landsat datasets, the general trend of thermal patterns in the river can be observed, but for daily basis study and analysis, Landsat datasets are not enough. The abrupt change in the temperature of the river can be observed near the three confluence points.

The efficiency of the given algorithm is primarily hampered by the uncertainties associated with temperature estimation from Landsat series satellite data. Several ambiguities are associated with the temperature calculation of river surface (Handcock et al. 2006; Ling et al. 2017). Other factors that affect temperature calculation accuracy are sensor calibration, instrument noise, and in-scene spectral variability from non-water materials (Kay et al., 2005; Lamaro et al., 2013). However, the extensive number of observations can help make the outcome robust and dynamic. It may be a conceivable technique to mitigate the effects brought about by the uncertainty in utilizing the Landsat time-series data.

As mentioned earlier, TIR images have poor resolution. It can only measure water temperature for broad rivers; in this work, the river considered for analysis varies roughly around 230 to 700 meters over the study stretch. With the help of image enhancement algorithms, the surface water temperature for narrow streams can also be computed very easily (Cherkeuer et al., 2005; Ling et al., 2017). The advanced water temperature estimation algorithms can also be applied to enhance the accuracy of the analysis of thermal patterns determined from Landsat-5 thermal images (120m spatial resolution) or Landsat-7 thermal images (60m spatial resolution) (Das et al., 2022). Changing climatic conditions would obviously result in changing water resources in the river basins, regions, and countries. The direction of these changes would determine the general strategy of population and economy water supply in the next century (Georgiyevsky, 1996). It could be stated that the process adopted for this analysis gives a helpful modus operandi to fill in the scanty in-situ observation of the surface temperature of the river. Besides, an expected climate change would evidently influence not only the value of natural water resources but also water demand, water use, and availability, depending to a large extent on

climatic conditions as well. This algorithm may also be applicable on a global level due to the global coverage of Landsat satellites